


H. LI 
A. FAROOQ
J.B. JEFFRIES
R.K. HANSON

Near-infrared diode laser absorption sensor for rapid measurements of temperature and water vapor in a shock tube

High Temperature Gasdynamics Laboratory, Department of Mechanical Engineering, Stanford University, Stanford, CA 94305, USA

Received: 2 May 2007/Revised version: 31 July 2007

Published online: 26 September 2007 • © Springer-Verlag 2007

ABSTRACT A fast-response (100 kHz) tunable diode laser absorption sensor is developed for measurements of temperature and H₂O concentration in shock tubes, e.g. for studies of combustion chemistry. Gas temperature is determined from the ratio of fixed-wavelength laser absorption of two H₂O transitions near 7185.60 cm⁻¹ and 7154.35 cm⁻¹, which are selected using design rules for the target temperature range of 1000–2000 K and pressure range of 1–2 atm. Wavelength modulation spectroscopy is employed with second-harmonic detection (WMS-2*f*) to improve the sensor sensitivity and accuracy. Normalization of the second-harmonic signal by the first-harmonic signal is used to remove the need for calibration and minimize interference from emission, scattering, beam steering, and window fouling. The laser modulation depth for each H₂O transition is optimized to maximize the WMS-2*f* signal for the target test conditions. The WMS-2*f* sensor is first validated in mixtures of H₂O and Ar in a heated cell for the temperature range of 500–1200 K (*P* = 1 atm), yielding an accuracy of 1.9% for temperature and 1.4% for H₂O concentration measurements. Shock wave tests with non-reactive H₂O–Ar mixtures are then conducted to demonstrate the sensor accuracy (1.5% for temperature and 1.4% for H₂O concentration) and response time at higher temperatures (1200–1700 K, *P* = 1.3–1.6 atm).

PACS 42.62.Fi; 42.55.Px; 42.60.Fc; 07.35.+k

1 Introduction

Detailed chemical mechanisms are required in the design of modern combustion systems to optimize fuel consumption and pollutant formation [1]. Chemical kinetics studies in the controlled pressure and temperature environment of shock tubes provide important reaction rate parameters needed for such mechanisms as well as validation of complete combustion mechanisms [2–5]. When the heat release of the post-shock chemistry is small compared to the heat capacity of the gas mixture, the temperature increase (due to chemical reactions) will be insignificant [5], and the post-shock (incident and reflected) temperatures are precisely given by the

measured shock velocity and the standard shock wave relations. However, it is desirable to test chemical mechanisms of combustible mixtures that provide significant heat release. For these chemical kinetics shock tube experiments, a temperature sensor with fast time response providing accurate temperature time histories would improve the quality of kinetic data. Here, we report the development and initial use of a tunable diode laser (TDL) sensor for non-intrusive measurements of gas temperature and H₂O concentration behind reflected shock waves, with a 100 kHz bandwidth, thus providing a new diagnostic tool to study the combustion mechanisms of hydrocarbon fuels over a wide range of conditions. In cases where H₂O is not naturally present or is not a reasonable additive, other infrared-active tracers such as CO₂ may be used instead.

TDL sensors based on absorption spectroscopy have been demonstrated for non-intrusive in situ measurements of temperature, pressure, species concentration, and flow velocity in various applications [6–15]. Most of these TDL sensors are based on direct absorption techniques due to the relatively simple interpretation of measurement results [6–12]. Gas temperature can be determined from the ratio of peak absorbance or spectrally integrated absorbance of two transitions with line strengths that exhibit different temperature dependences due to differences in lower-state energy. For scanned-wavelength direct absorption measurements, high-resolution absorption line shapes are recorded by scanning the laser wavelength across the absorption features. The sensor bandwidth is usually limited to several kHz by the wide laser scanning range needed to reach the non-absorbing wings of the spectroscopic features, in order to infer the zero-absorption baseline. A fixed-wavelength direct absorption technique may be used to improve the sensor bandwidth [8]. However, these direct absorption methods can be prone to errors for low-absorption applications because of various noise sources such as beam steering and chemiluminescent emission.

Wavelength modulation spectroscopy (WMS), as an extension of absorption spectroscopy, is a well-known technique for improving the signal-to-noise ratio (SNR) [12–22]. In this technique, the laser wavelength is rapidly modulated (typically hundreds of kHz), and the second harmonic of the laser transmission signal (WMS-2*f* signal) is recorded by a lock-in amplifier. Gas temperature can be inferred from the ratio of

✉ Fax: +1-650-723-1748, E-mail: hejieli@stanford.edu

the WMS- $2f$ signals of two transitions [12–14, 18–21]. This technique is sensitive to absorption line shape curvature rather than the absorption magnitude alone, and is insensitive to low-frequency noise. Thus, WMS- $2f$ offers benefits over direct absorption in terms of noise resistance and sensitivity. For example, in the case of weak absorbance, the baseline fitting which is required in the scanned-wavelength direct absorption measurements is a large source of uncertainty. This problem is eliminated in the WMS measurements. The lock-in amplifier also serves as a band-pass filter and rejects noise outside the lock-in bandwidth. Finally, normalization of the WMS- $2f$ signal with the $1f$ signal can remove the need for calibration and account for the laser transmission variations due to beam steering, scattering, and window fouling. Such normalization was first introduced in 1982 [11], and its utility was recently shown in [20–24]. These benefits make WMS with second-harmonic detection an attractive technique for combustion measurements. Scanned-wavelength WMS- $2f$ has been successfully demonstrated in various applications [12–15] with typical bandwidth of several kHz; a fixed-wavelength WMS- $2f$ technique has been demonstrated in IC engines with a bandwidth of 7.5 kHz [21]. In shock tube studies of combustion mechanisms of hydrocarbon fuels, the typical test time ranges from several tens of microseconds to a few milliseconds, so that the desired sensor bandwidth is at least 100 kHz. Hence, fixed-wavelength WMS- $2f$ is used in our TDL sensor design to achieve the needed high bandwidth. To our knowledge, this is the first realization of a temperature sensor with 100 kHz bandwidth using a WMS- $2f$ technique.

Water vapor is a major combustion product of hydrocarbon fuels and has a strong and broad absorption spectrum. Furthermore, the rovibrational spectrum of water vapor in the near infrared (NIR) overlaps with well-developed telecommunication laser technology [6]. Therefore, H_2O has been chosen as the target absorbing species to be probed in these initial shock tube experiments. In subsequent applications, gas temperature inferred from the absorption ratio of two H_2O transitions can provide useful information of heat release, while the H_2O concentration will serve to indicate the completeness of combustion.

In this work, a fast-response (100 kHz) NIR diode laser absorption sensor based on fixed-wavelength WMS- $2f$ is developed to measure gas temperature and H_2O concentration in a shock tube, in anticipation of its use in studies of combustion kinetics. The absorption transitions of H_2O in the 1.3–1.5 μm region are first systematically analyzed to select the optimum line pair for the target temperature range of 1000–2000 K and pressure range of 1–2 atm. Two H_2O transitions near 7185.60 cm^{-1} and 7154.35 cm^{-1} are selected for the TDL sensor with the criteria of strong absorption strength, relatively small interference from ambient H_2O , and good isolation from neighboring transitions. The laser modulation depth for each H_2O transition is optimized to maximize the WMS- $2f$ signal for the targeted shock tube test conditions and to simplify signal interpretation. The TDL sensor for temperature and H_2O concentration measurements is first validated in a heated static cell (500–1200 K) containing H_2O –Ar mixtures. Shock tube tests with non-reactive H_2O –Ar mixtures are then used to demonstrate the sensor accuracy and response time at combustion temperatures (1200–1700 K).

2 Fundamental spectroscopy

The theory of WMS including real diode laser performance has been described in detail previously [20]. Here, we present the related principles for the TDL sensor development. For fixed-wavelength WMS- $2f$ detection of absorption, the diode laser injection current is sinusoidally modulated with angular frequency $\omega = 2\pi f$, and the instantaneous laser output frequency $\nu(t)$ can be expressed by

$$\nu(t) = \bar{\nu} + a \cos(\omega t), \quad (1)$$

where $\bar{\nu}$ [cm^{-1}] is the center laser frequency and a [cm^{-1}] is the modulation depth. The diode laser intensity is simultaneously modulated:

$$I_0(t) = \bar{I}_0 [1 + i_0 \cos(\omega t + \psi_1) + i_2 \cos(2\omega t + \psi_2)]. \quad (2)$$

Here, \bar{I}_0 is the average laser intensity at $\bar{\nu}$, i_0 is the linear intensity modulation (IM) amplitude with phase shift ψ_1 , and i_2 is the nonlinear IM amplitude with phase shift ψ_2 [17, 19, 20].

The transmission coefficient $\tau(\nu)$ of monochromatic radiation through a uniform gas medium of length L [cm] is described by the Beer–Lambert relation

$$\tau(\nu) = \left(\frac{I_t}{I_0} \right)_\nu = \exp[-\alpha(\nu)]. \quad (3)$$

Here, I_t and I_0 are the transmitted and incident laser intensities, respectively. Also, $\alpha(\nu)$ represents the spectral absorbance

$$\alpha(\nu) = P \chi_i S(T) \varphi_\nu L, \quad (4)$$

where P [atm] is the total gas pressure, χ_i is the mole fraction of the absorbing species, S [$\text{cm}^{-2}/\text{atm}$] and φ_ν [cm] are the line strength and line shape function for the absorption feature, and T [K] is the gas temperature. The transmission coefficient is a periodic even function in ωt and can be expanded in a Fourier cosine series:

$$\tau[\bar{\nu} + a \cos(\omega t)] = \sum_{k=0}^{\infty} H_k(\bar{\nu}, a) \cos(k\omega t), \quad (5)$$

where the components $H_k(\bar{\nu}, a)$ are given by

$$H_0(\bar{\nu}, a) = \frac{1}{2\pi} \int_{-\pi}^{\pi} \tau(\bar{\nu} + a \cos \theta) d\theta, \quad (6)$$

$$H_k(\bar{\nu}, a) = \frac{1}{\pi} \int_{-\pi}^{\pi} \tau(\bar{\nu} + a \cos \theta) \cos k\theta d\theta. \quad (7)$$

For WMS- $2f$ detection, a lock-in amplifier is used to measure the second-harmonic ($2f$) signal by multiplying the detector signal by a sinusoidal reference signal at frequency 2ω . The magnitude of the WMS- $2f$ signal can be written as [20]

$$\begin{aligned} R_{2f}(\bar{\nu}) &= \frac{G \bar{I}_0}{2} \left\{ \left[H_2 + \frac{i_0}{2} (H_1 + H_3) \cos \psi_1 \right. \right. \end{aligned}$$

$$\begin{aligned}
 & +i_2 \left(H_0 + \frac{H_4}{2} \right) \cos \psi_2 \Big]^2 \\
 & + \left[\frac{i_0}{2} (H_1 - H_3) \sin \psi_1 + i_2 \left(H_0 - \frac{H_4}{2} \right) \sin \psi_2 \right]^2 \Big]^{1/2}, \quad (8)
 \end{aligned}$$

where G accounts for the optical–electrical gain of the detection system and the laser transmission losses due to scattering, beam steering, and window fouling [14, 20]. When there is no absorption, $H_0 = 1$ and $H_k = 0$ (for $k > 0$), so that (8) reduces to $R_{2f}^0 = G\bar{I}_0 i_2/2$. This background $2f$ signal comes from the nonlinear laser IM, and is often referred to as the residual amplitude modulation (RAM) [17, 19, 20]. In WMS measurements, the background $2f$ signal needs to be measured in the absence of absorption and vector subtracted from the $2f$ signal. The magnitude of the absorption-based WMS- $2f$ signal is then given by

$$\begin{aligned}
 & S_{2f}(\bar{\nu}) \\
 & = \frac{G\bar{I}_0}{2} \left\{ \left[H_2 + \frac{i_0}{2} (H_1 + H_3) \cos \psi_1 \right. \right. \\
 & \quad \left. \left. + i_2 \left(H_0 - 1 + \frac{H_4}{2} \right) \cos \psi_2 \right]^2 \right. \\
 & \quad \left. + \left[\frac{i_0}{2} (H_1 - H_3) \sin \psi_1 + i_2 \left(H_0 - 1 - \frac{H_4}{2} \right) \sin \psi_2 \right]^2 \right\}^{1/2}. \quad (9)
 \end{aligned}$$

For the small modulation depths ($a \sim 0.06 \text{ cm}^{-1}$, $i_2 \sim 0.002$, $i_0 \sim 0.26$) used in this work, the contribution of nonlinear laser IM to the absorption-based WMS- $2f$ signal near the line center of discrete spectra can be neglected, and the phase shift ψ_1 can be assumed to be π [20]. Equation (9) is thus reduced to the commonly used simple model [12–16]

$$S_{2f}(\bar{\nu}) = \frac{G\bar{I}_0}{2} \left| H_2 - \frac{i_0}{2} (H_1 + H_3) \right|. \quad (10)$$

Similarly, the magnitude of the first-harmonic ($1f$) signal can be obtained as

$$S_{1f}(\bar{\nu}) = \frac{G\bar{I}_0}{2} \left| H_1 - i_0 \left(H_0 + \frac{H_2}{2} \right) \right|. \quad (11)$$

In the limit of no absorption, the WMS- $1f$ signal is reduced to $S_{1f}^0 = G\bar{I}_0 i_0/2$, which is generated by the linear IM. Figure 1 illustrates the first four Fourier components obtained for the H_2O line near 7185.60 cm^{-1} for $P = 1.5 \text{ atm}$, $0.5\% \text{ H}_2\text{O}$ in Ar, and $L = 15 \text{ cm}$. It can be seen that H_1 and H_3 are zero valued and H_2 is maximized at line center in the case of an isolated absorption feature. Thus, the second Fourier component, H_2 , is the dominant term for the WMS- $2f$ signal near line center. In addition, H_0 is close to unity, and is the dominant term for the WMS- $1f$ signal near line center (close to $G\bar{I}_0 i_0/2$).

The hardware-related parameters and transmission losses can thus be accounted for by normalizing the absorption-based WMS- $2f$ signal with the WMS- $1f$ signal [20]:

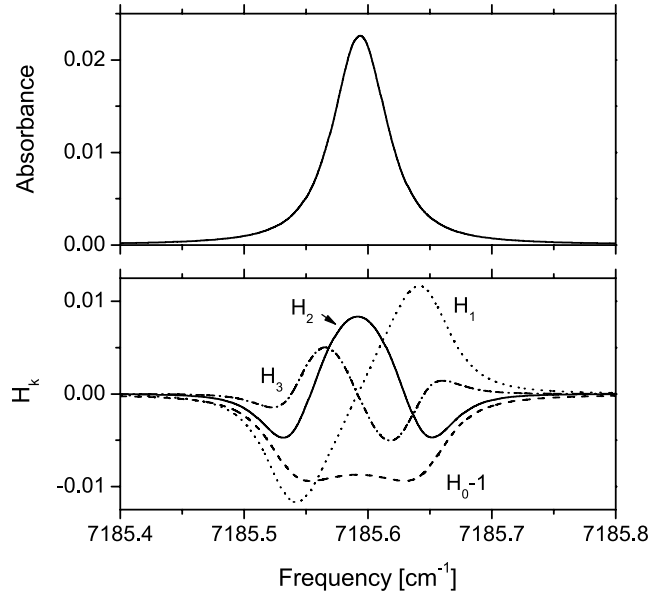


FIGURE 1 Simulated absorption line shape for the H_2O line near 7185.60 cm^{-1} and the corresponding coefficients H_k in the Fourier cosine series for $P = 1.5 \text{ atm}$, $0.5\% \text{ H}_2\text{O}$ in Ar, $L = 15 \text{ cm}$, and $a = 0.058 \text{ cm}^{-1}$. Neighboring features have been neglected

$$C = \frac{S_{2f}}{S_{1f}} = \frac{|H_2 - i_0 (H_1 + H_3)/2|}{|H_1 - i_0 (H_0 + H_2/2)|}. \quad (12)$$

By this normalization, common terms such as the laser intensity, detector sensitivity, signal amplification, lock-in gain, and laser transmission variations are eliminated. The $1f$ -normalized WMS- $2f$ signal, C , is a function of laser parameters (i_0 , a) and gas parameters (P , T , χ_i) only. The laser parameters can be determined before the measurements. Therefore, no calibration is needed to scale the simulations to the measurements [20].

For optically thin samples ($\alpha(\nu) < 0.1$), the transmission coefficient can be approximated as

$$\tau(\nu) = \exp[-\alpha(\nu)] \approx 1 - \alpha(\nu) = 1 - P\chi_i S\varphi_\nu L, \quad (13)$$

and the k th-harmonic Fourier component simplifies as

$$H_k(\bar{\nu}, a) = -\frac{SP\chi_i L}{\pi} \int_{-\pi}^{\pi} \varphi(\bar{\nu} + a \cos \theta) \cos k\theta d\theta. \quad (14)$$

Therefore, the WMS- $2f$ signal is directly proportional to the line strength $S(T)$ and species concentration χ_i when the line shape functions do not vary for the range of conditions found in the applications [20]. Note that in addition to the absorption parameters, the WMS- $2f$ signal also depends on the modulation depth a . The WMS- $2f$ signal can be maximized by choosing the optimum modulation index m to be ~ 2.2 , which is defined as

$$m = \frac{a}{\Delta\nu/2}, \quad (15)$$

where $\Delta\nu [\text{cm}^{-1}]$ is the full width at half maximum (FWHM) of the absorption line shape [14, 16, 25].

Gas temperature can be obtained from the ratio of the $1f$ -normalized WMS- $2f$ signals near the line center of two transitions

$$R = \frac{C_2}{C_1} = \frac{(S_{2f}/S_{1f})_{\bar{\nu}_2}}{(S_{2f}/S_{1f})_{\bar{\nu}_1}}, \quad (16)$$

which is closely related to the ratio of absorption line strengths. If the total gas pressure is measured by a pressure transducer, the gas temperature can be inferred from the measured ratio R , using simulations of the ratio as a function of temperature at the measured pressure. The simulations using (12) and (16) include the effects of differences in line shape function (between the two lines) owing to different values of laser modulation parameters and broadening coefficients. After the temperature is known, the species concentration can be determined from either of the $1f$ -normalized WMS- $2f$ signals.

3 Sensor design

3.1 Selection of spectral lines

Selection of optimum absorption transitions is the first important step in the development of two-line thermometry based on WMS- $2f$ detection. Systematic line-selection criteria for absorption-based thermometry have been developed in the literature [27, 28]. Here, we briefly discuss the design rules to evaluate the choices and choose the optimum H₂O lines for combustion temperature measurements in near-atmospheric-pressure shock tube experiments. This procedure is similar to that used in [28] and can be extended to high-pressure applications [29].

The first criterion employed in the present study is to limit the wavelength range to the spectral region of 1.3–1.5 μm , where the $2\nu_1$, $2\nu_3$, and $\nu_1 + \nu_3$ bands of the H₂O absorption spectrum overlap with the telecommunication band. In this region, robust fiber-coupled single-mode diode lasers and fiber optics are readily available. There are 6435 H₂O lines listed in the HITRAN 2004 database [30] within this region.

The second criterion is to ensure sufficient absorption for high-SNR measurements over the expected conditions in the shock tube: $T = 1000$ – 2000 K, $P = 1$ – 2 atm, $\chi_{\text{H}_2\text{O}} = 0.001$ – 0.02 , and $L = 15$ cm. Here, we assume a minimum detectable absorbance of 0.0002 (which is estimated from the actual WMS- $2f$ experiments) and a desired SNR ≥ 10 . Thus, the peak absorbance is required to be larger than 0.002. The line center absorption for each H₂O transition in the 1.3–1.5 μm region is calculated with the spectroscopic parameters provided by HITRAN 2004, and is found to be less than 0.12 for the expected conditions. Thus, no upper limit for the peak absorption is necessary for our sensor design. This criterion reduces the possible lines from 6435 to 139 potential candidates.

The third criterion is to minimize the absorption interference from ambient water vapor. For a H₂O transition with strong absorption at room temperature (i.e. with a small value of lower-state energy E''), great care must be taken in purging the region outside the target measurement path length with nitrogen or dry air [26]. This difficulty can be mitigated by using H₂O transitions with lower-state energy $E'' >$

1000 cm^{-1} . This criterion reduces the number of candidate lines to 90.

The fourth criterion is freedom of significant interference from nearby transitions to minimize the uncertainty in the analysis of WMS- $2f$ measurements over the expected conditions in the shock tube. We simulate the absorption spectra for the remaining 90 candidates at $T = 1000$ K and 2000 K, $P = 1.5$ atm, with the parameters from HITRAN 2004 to investigate the potential interference from neighboring transitions. Only features free from strong interferences within $\pm 0.3 \text{ cm}^{-1}$ of their line center frequencies are retained. This criterion reduces the number of candidate transitions to 17.

For WMS- $2f$ measurements, accurate information of the spectral line shapes and their temperature dependences is needed. The HITRAN 2004 database provides a good reference for sensor design. However, the spectroscopic parameters of the selected transitions must be validated before use in a combustion sensor. In addition, some spectral parameters are not listed in the HITRAN database: temperature exponents for self-broadening and shift parameters, Ar-broadening and -narrowing parameters [31]. Experiments in a well-controlled environment (e.g. a heated static cell with temperature up to 1200 K) are usually conducted to determine these important spectroscopic parameters [26–28, 31]. Thus, the fifth criterion, to be free of significant interference from nearby transitions for the temperature range of 500 – 1200 K, minimizes the uncertainty in the measurements of spectroscopic parameters in the heated static cell. This criterion further reduces the number of candidate transitions to five as listed in Table 1.

Figure 2 shows the simulated H₂O (0.5%) absorption spectra for the five selected lines based on HITRAN 2004 parameters. It can be seen from Fig. 2 that lines C, D, and E are weaker than lines A and B for the target temperature range of 1000 – 2000 K. Therefore, the two H₂O transitions near 7154.35 cm^{-1} (line A) and 7185.60 cm^{-1} (line B) are selected for the WMS- $2f$ temperature sensor to optimize the SNR in shock tube measurements. If the absorbance is larger (i.e. in applications with higher water concentration or longer path length), the line pair BE could be employed to improve the temperature sensitivity for high-temperature measurements ($T \sim 2000$ K).

The spectroscopic parameters for the two selected H₂O transitions have been systematically measured in a heated static cell and are summarized in Table 2 (all data are taken from [31]). The measured high-resolution Ar-broadened H₂O absorption line shapes deviated significantly from the commonly used Voigt profile because of collisional narrowing [32–34]. Therefore, the Galatry line shape function [33] has been utilized to include the collisional-narrowing effects

Line	Wavelength [nm]	Frequency [cm^{-1}]	$S(296 \text{ K})$ [$\text{cm}^{-2}/\text{atm}$]	E'' [cm^{-1}]
A	1397.75	7154.35	3.85E-4	1789.04
B	1391.67	7185.60	1.97E-2	1045.06
C	1342.11	7450.93	5.38E-4	1690.66
D	1341.48	7454.44	1.83E-4	1962.51
E	1339.08	7467.77	1.27E-5	2551.48

TABLE 1 Candidate H₂O lines for NIR TDL sensor for shock tube. Line selection based on the HITRAN 2004 database

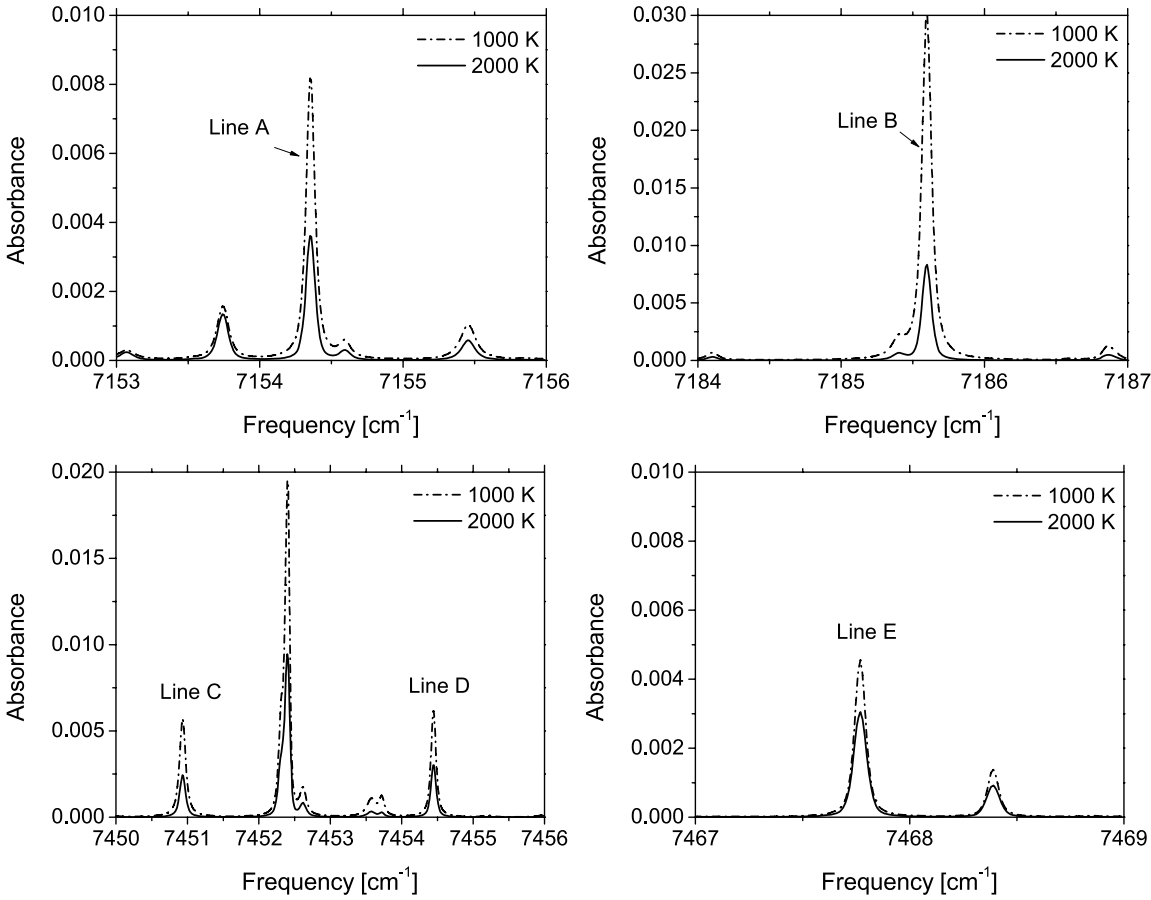


FIGURE 2 Simulated absorption spectra for the five selected H₂O lines in the 1.4 μm region using the HITRAN 2004 database for $P = 1.5$ atm, 0.5% H₂O in air, $L = 15$ cm

induced by Ar–H₂O collisions. Note that the Galatry profile is computationally more expensive than the relatively simple Voigt profile [34]. We refer the reader to [31] for a detailed discussion. Figure 3 plots the measured line strength versus temperature for these two H₂O transitions.

3.2 Optimization of modulation depth

As can be seen from (14), the WMS-2*f* peak height is dependent on the line shape function, which can potentially cause difficulties in the temperature measurements using WMS-2*f* spectroscopy. Fortunately, this effect can be mitigated by choosing the optimum modulation depth, as discussed in [14].

Figure 4 plots the simulated WMS-2*f* peak height (which is essentially the normalized value of the integral in (14) for H₂) of the H₂O transition near 7185.60 cm⁻¹ versus modulation depth at three temperatures ($T = 1000, 1500,$ and

2000 K; $P = 1.5$ atm, 1% H₂O in Ar, and $L = 15$ cm). The Galatry line shape function with the spectroscopic parameters listed in Table 2 is used in the numerical simulation. For these conditions, the FWHM of the absorption line shape is ~ 0.052 cm⁻¹. The maximum values of the WMS-2*f* peak signal occur at modulation index $m \sim 2.2$ for all three temperatures, which is consistent with previous work using Gaussian, Lorentzian, and Voigt line shapes [14, 16, 25]. Furthermore, the WMS-2*f* peak height varies very slowly for modulation depths with m near 2.2. By choosing the optimum modulation depth $a_{\text{opt}} = 0.058$ cm⁻¹ with $m = 2.2$ at $T = 1500$ K and $P = 1.5$ atm, the integral in (14) remains relatively constant for the target temperature range of 1000–2000 K. Thus, the ratio of two WMS-2*f* peak heights is mainly a function of the well-known line strengths of the selected absorption features. Similarly, the optimum modulation depth for the H₂O transition near 7154.35 cm⁻¹ is determined to be 0.055 cm⁻¹ for the range of expected test conditions in the shock tube. These

ν_0 [cm ⁻¹]	$S(296\text{ K})$ [cm ⁻² /atm]	E'' [cm ⁻¹]	$\gamma_{\text{self}}(296\text{ K})$ [cm ⁻¹ /atm]	n_{self}	$\gamma_{\text{Ar}}(296\text{ K})$ [cm ⁻¹ /atm]	n_{Ar}	$\beta_{\text{Ar}}(296\text{ K})$ [cm ⁻¹ /atm]	N	$\delta_{\text{Ar}}(296\text{ K})$ [cm ⁻¹ /atm]	m
7185.60	1.91E-2	1045.1	0.205	0.59	0.0176	0.40	0.0407	0.59	-0.0213	1.07
7154.35	3.67E-4	1789.0	0.151	0.65	0.0145	0.36	0.0343	0.56	-0.0241	1.11

Note: $\gamma(T) = \gamma(296\text{ K})(296/T)^n$, $\beta(T) = \beta(296\text{ K})(296/T)^N$, $\delta(T) = \delta(296\text{ K})(296/T)^m$

TABLE 2 Measured spectroscopic data (based on a Galatry profile) for the selected H₂O line pair for the TDL sensor. All data taken from [31]

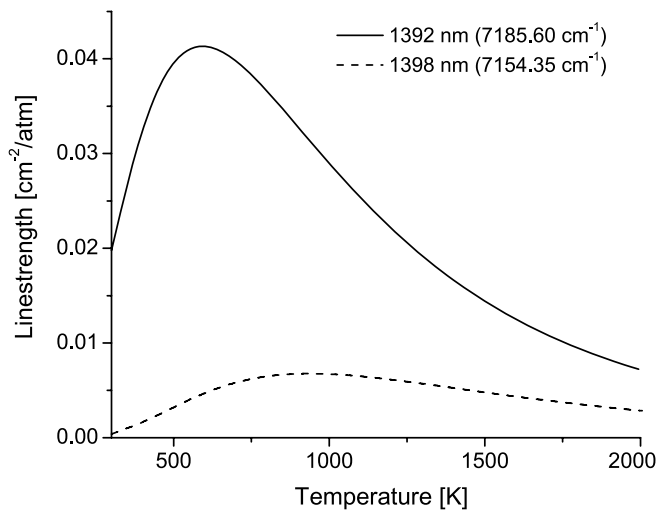


FIGURE 3 Line strength as a function of temperature for H₂O lines at 1392 nm and 1398 nm, using validated parameters taken from [31] (see Table 2)

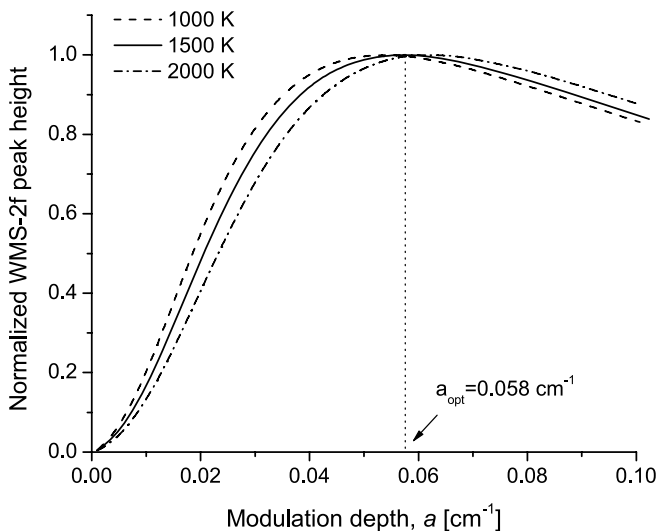


FIGURE 4 Simulated WMS-2*f* peak height for the H₂O transition near 7189.60 cm⁻¹ versus modulation depth *a*; *P* = 1.5 atm, 1% H₂O in Ar, and *L* = 15 cm

selected modulation depths are suitable for WMS measurements in the pressure range of 1.2–1.8 atm and temperature range of 1000–2000 K. For significantly different pressures and temperatures, different modulation depths can be determined using the same procedure.

For the fixed-wavelength WMS-2*f* sensor, the laser wavelengths are chosen near the line center of the two H₂O transitions, and gas temperature is determined by comparison of the measured WMS-2*f* signal ratio with simulations at the measured pressure by a pressure transducer. Figure 5 illustrates the simulated WMS-2*f* signal ratio for the 7154.35 cm⁻¹/7185.60 cm⁻¹ line pair as a function of temperature for various pressures with optimum modulation depths for the two H₂O transitions (1% H₂O in Ar). The WMS-2*f* signal ratio is closely related to the ratio of absorption line strengths, and is only a weak function of pressure. For example, at *T* = 1300 K, a 12.5% change in total gas pressure

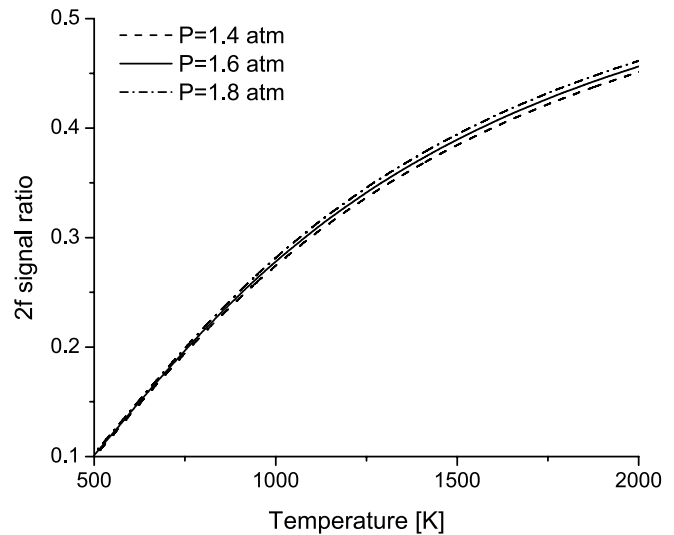


FIGURE 5 Simulated WMS-2*f* signal ratio for 7154.35 cm⁻¹/7185.60 cm⁻¹ line pair as a function of temperature for various pressures; 1% H₂O in Ar, modulation depth *a* = 0.055 cm⁻¹ and 0.058 cm⁻¹ for lines 7154.35 cm⁻¹ and 7185.60 cm⁻¹, respectively

induces only a small change (1.3%) in the inferred gas temperature. Thus, the changes in the measured WMS-2*f* ratio primarily reflect the changes of gas temperature.

4 Sensor validation in heated cell

4.1 Experimental setup

The TDL sensor is first validated in a three-section heated static cell with an inner diameter of 4.4 cm, before being used in shock-heated gases. Figure 6 illustrates the experimental setup, which has also been used for the spectroscopy measurements of the two H₂O transitions used in the TDL sensor [31]. The temperature in the center section of the quartz cell is accurately controlled by a three-zone furnace (MHI H14HT 2.5 × 27) with three independently adjustable heaters. The center section of the cell is filled with a H₂O–Ar test mixture, while the outer sections are in vacuum to avoid interference from ambient water vapor. The cell has wedged (2.5°) windows to avoid interference effects as the laser wavelength is modulated. Three type-K thermocouples (Omega) with an accuracy of ±0.75% of reading are equally spaced along the center section of the cell to measure the temperature of gas samples. At each temperature set point up to 1200 K, the maximum temperature difference is < 0.5%. The gas pressures are measured by a 1000 Torr (1 Torr = 1/760 atm) MKS Baratron pressure transducer with an accuracy of ±0.12% of reading. To prepare the H₂O–Ar mixture, pure water vapor and Ar are sequentially introduced into a stainless steel tank with teflon beads, producing a mixture with ~ 1% H₂O in Ar. The tank is first shaken and then allowed to settle for at least 12 h before the H₂O–Ar mixture is used for the experiments.

Two fiber-coupled distributed-feedback (DFB) diode lasers (NEL NLK1E5E1AA, 10 mW) operating near 1392 nm and 1398 nm are multiplexed into a single-mode fiber. Each laser is mounted in a commercial laser mount (ILX Lightwave LDM-4980) and maintained at constant temperature

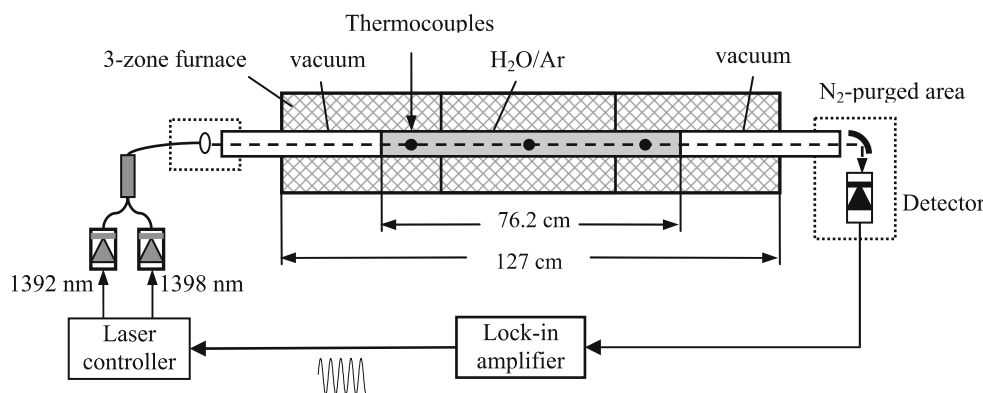


FIGURE 6 Schematic of the experimental setup used for WMS-2*f* sensor validation

(ILX Lightwave LDT-5910). The laser center wavelengths are tuned to 1391.673 nm (7185.596 cm^{-1}) and 1397.751 nm (7154.350 cm^{-1}), respectively, using a Burleigh WA-100 wavemeter. These two wavelengths are near the line center of the two H_2O transitions for the test conditions [31]. Each laser wavelength is modulated by a sinusoidal current modulation: $f = 200\text{ kHz}$ and $a = 0.062\text{ cm}^{-1}$ for laser 1392 nm, $f = 550\text{ kHz}$ and $a = 0.057\text{ cm}^{-1}$ for laser 1398 nm. The laser modulation depths are inferred by sinusoidally fitting the fringe centers in the interference pattern produced by a fiber-optic etalon with a free spectral range of 0.0277 cm^{-1} . These modulation depths are adjusted to the optimal values for cell conditions. The amplitude of laser IM (i_0) is determined by fitting the laser intensity signal without absorption. The laser beam is collimated by a lens (Thorlabs F220FC-C), directed across the cell, and focused by a spherical mirror onto an In-GaAs detector (Thorlabs PDA 400, 10 MHz). The optics and detector are enclosed by plastic bags purged by dry N_2 to avoid absorption interference from ambient water vapor. The residual H_2O is negligible in the bag as the quality of the purging is checked by direct absorption before measurements. The detector signal is demodulated by a Perkin-Elmer lock-in amplifier (model 7280) to recover the $1f$ and $2f$ signals with a time constant of $10\text{ }\mu\text{s}$.

In the validation tests, the diode lasers are turned on one at a time to probe the two H_2O transitions. The heated static cell is first evacuated and the background $1f$ signal (magnitude S_{1f}^0) and $2f$ signal (X and Y components for vector subtraction, see (8) and (9)) are taken for each laser. The cell is then filled with H_2O -Ar mixture to $P = 1\text{ atm}$, and the $1f$ and $2f$ signals with absorption are recorded for each laser. The background-subtracted $1f$ -normalized WMS-2*f* signal is compared with simulations (Fig. 5) to infer gas temperature and H_2O concentration in the cell. The background $2f$ signal is less than 1.5% and 8% of the absorption-based $2f$ signal for lasers 1392 and 1398 nm, respectively. The 1392 nm laser is injection current tuned with a 100 Hz linear ramp (with sinusoidal modulation off) across the absorption feature near 7185.60 cm^{-1} to determine the actual H_2O concentration in the test mixture for comparison.

4.2 Results

Figure 7 shows the measured H_2O absorption spectrum in the H_2O -Ar mixture at the experimental conditions of $T = 1047\text{ K}$, $P = 1\text{ atm}$. The experimental profiles are best-fit

using a Galatry profile [31], and the residual (difference between data and fit normalized by peak absorbance) is shown in the upper panel. The H_2O mole fraction in this test mixture is inferred to be 0.0105 using the integrated absorbance area for the H_2O transition near 7185.60 cm^{-1} with the line strength data listed in Table 2. The H_2O concentration varies (by up to $\pm 5\%$) from one fill to another due to adsorption in the mixing tank and the gas handling system [35].

The left-hand panel of Fig. 8 compares the thermocouple measurements with the temperatures from the WMS-2*f* sensor measurements (sensor bandwidth 100 kHz, no averaging). The temperatures determined from the WMS-2*f* sensor are in good agreement with the thermocouple readings (standard deviation = 1.9%) over the entire temperature range of 500–1200 K. The right-hand panel of Fig. 8 shows the ratio of the H_2O mole fraction measured by the WMS-2*f* sensor using the high- E'' line at 7154.350 cm^{-1} (χ_{Measured}) and the mole fraction measured by direct absorption with the transition near 7185.60 cm^{-1} (χ_{Actual}). The standard deviation between the measured and actual H_2O mole fractions is 1.4% over the tested temperature range. The excellent agreement between measured and actual values confirms the accuracy

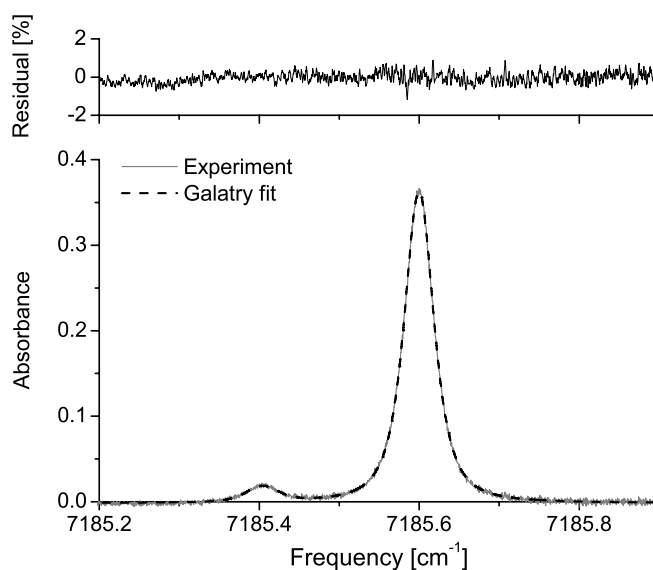


FIGURE 7 Measured absorption spectrum in the heated cell with $P = 1\text{ atm}$ and $T = 1047\text{ K}$. A least-squares two-line Galatry fit yields $X_{\text{H}_2\text{O}} = 0.0105$. The residual is the difference between data and fit normalized by peak absorbance

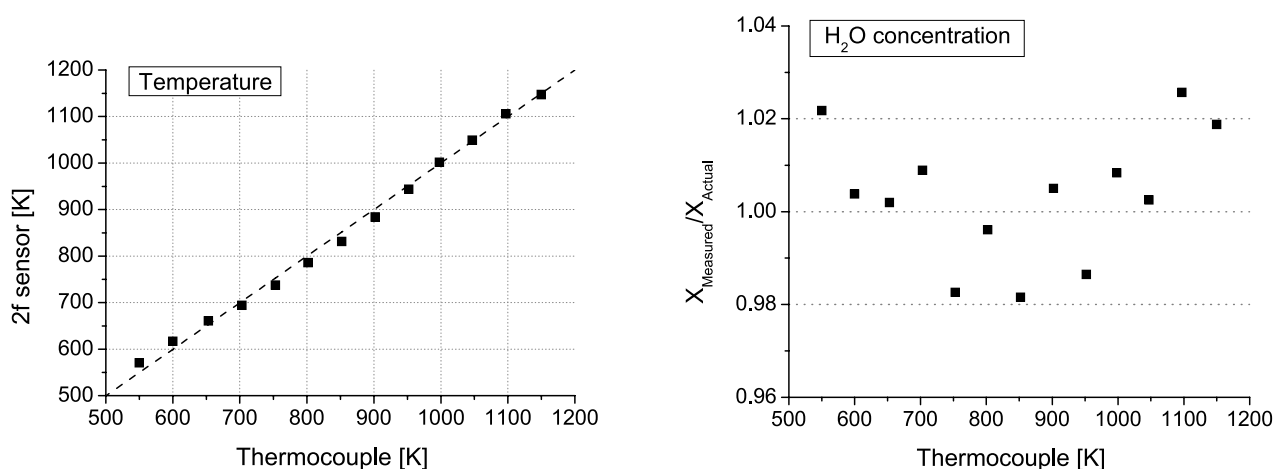


FIGURE 8 Validation measurements of the TDL WMS-2f sensor in the well-controlled static cell. $P = 1$ atm, $\sim 1.0\%$ H₂O in Ar, $L = 76.2$ cm

of the WMS-2f sensor for both temperature and H₂O concentration measurements. The errors in Fig. 8 primarily come from the uncertainties in the measured spectroscopic data (3%), temperature measurements by thermocouple (0.75%), and errors in the baseline and profile fits (0.5%) in the direct absorption measurements.

5 Measurements in H₂O/Ar shocks

5.1 Experimental setup

To illustrate the potential of the WMS-2f sensor for monitoring gas temperature and H₂O concentration in studies of the combustion mechanisms of hydrocarbon fuels, shock tube tests were conducted with dilute H₂O–Ar mixtures to validate the sensor accuracy and response at combustion temperatures. Figure 9 is a schematic of the experimental setup. Experiments were performed behind reflected shock waves in a helium-pressure-driven stainless-steel shock tube, which has been used in previous studies of reaction kinetics [36, 37]. The driven section is 10.5-m long and has an inner diameter of 15.24 cm. Incident shock velocities are measured over four intervals using five piezoelectric pressure transducers (PCB model 11A36) and four counters (Fluke PM6666), allowing accurate determination of the velocity at the shock tube end wall. The pre-shock initial mixture pressure is measured using a 100 Torr MKS Baratron pressure transducer. Reflected shock temperature is calculated from these measured velocities and one-dimensional shock wave relations, assuming vibrational equilibrium and frozen chemistry. The estimated uncertainty in reflected shock temperature is less than ± 20 K at 2000 K [36].

TDL measurements are made at a location 2 cm from the end wall. The two diode lasers near 1392 nm and 1398 nm are sinusoidally modulated by 400 kHz digital waveforms generated by a PC running a 10 MHz National Instruments data-acquisition (NI-DAQ) system. The NI-DAQ system consists of a PCI-6115 DAQ board (12-bit A/D conversion) and a BNC-2110 analog I/O block. The modulation depths are adjusted close to the optimal values (Sect. 3.2): $a = 0.059$ cm⁻¹ for laser 1392 nm and 0.056 cm⁻¹ for laser 1398 nm. The corresponding laser intensity modulation amplitude is $i_0 = 0.26$ for both lasers. The light from each laser is collimated, trans-

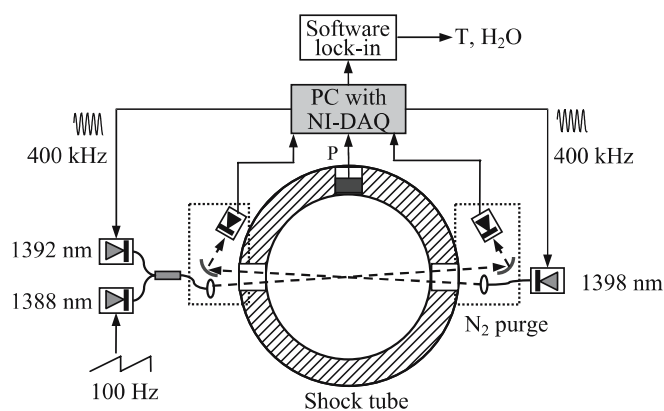


FIGURE 9 Experimental setup for shock tube measurements with the WMS-2f sensor

mitted through the shock tube with opposite directions, and focused onto an InGaAs detector (PDA 400). This optical configuration is based on the assumption that the gas properties across the shock tube are uniform. The H₂O concentration in the initial test mixture is determined by direct absorption before the shock for comparison. For this, an additional laser near 1388 nm is used to scan over an absorption feature near 7205.25 cm⁻¹, which is strong at room temperature ($S(296$ K) = 0.246 cm⁻²/atm) [38]. The optics and detectors are enclosed in plastic bags purged by dry N₂. The detector signals are recorded at 10 MHz using the same computer. The detector signal is demodulated by a digital lock-in program [14, 20, 22] on LabVIEW with a low-pass filter bandwidth of 100 kHz to extract the 1f and 2f (X and Y component) signals. An additional Kistler transducer is used to record the pressure time history at the same location during shock tests.

The test procedure is similar to the one described earlier in Sect. 4. Prior to each experiment, the shock tube is evacuated by a turbomolecular pump. The background 1f signal and 2f signal are taken for the lasers 1392 and 1398 nm, and the baseline signal for a direct absorption scan of laser 1388 nm is also taken (with laser 1392 nm off). The shock tube is then filled with the H₂O–Ar mixture to $P_1 = 0.04$ –0.08 atm. The direct absorption scan for laser 1388 nm is recorded and normalized with the baseline signal to infer the H₂O mole fraction

(χ_{Actual}). The laser 1388 nm is then turned off and the laser 1392 nm is turned on. The DAQ system is triggered by the pressure transducer to record pressure and transmission signals for both the 1392 and 1398 nm lasers during the shock heating to infer the time history of gas temperature and H_2O concentration.

5.2 Results

Figure 10 shows the measured time history of pressure and temperature during a shock with initial H_2O –Ar mixture at $P_1 = 0.08$ atm and $T_1 = 295$ K. The WMS-2*f* sensor is seen to have a fast response and a good SNR for temperature measurements. The rise time of the sensor is ~ 6 μs , which approaches the time for the ~ 1 mm/ μs reflected shock wave to cross the 2-mm-diameter laser beam. The average measured temperature over the time interval 0.1–1 ms (where T and P are expected to be virtually constant) is 1226 K with a standard deviation (i.e. fluctuation) of 14 K (1.1%). This is in excellent agreement (within 1.2%) with the value calculated from the ideal shock relations, $T_5 = 1211$ K. The sensor can also measure the gas temperature after the arrival of the rarefaction wave at about 1.85 ms. The temperature measurement by the WMS-2*f* sensor is not sensitive to the noise in the measured pressure (as discussed in Sect. 3.2). Thus, the noise in the temperature measurement mostly comes from the laser and detection system. Figure 11 plots the measured H_2O mole fraction during the same shock test with the WMS-2*f* sensor. The average value measured by both lasers is 0.00702 with a standard deviation of 0.00014. This is in good agreement (within 1.7%) with the direct absorption measurement (0.0069) before the shock. The scatter on the H_2O concentration in Fig. 11 comes from the noise in the individual laser signals as well as in the measured temperature and pressure (Fig. 10). If the calculated values of T_5 and P_5 are used instead of the measured temperature and pressure, the inferred H_2O mole fraction recovers the expected value with a smaller scatter (0.00008).

Similar tests were performed at different temperatures. The left-hand panel of Fig. 12 provides comparisons of the

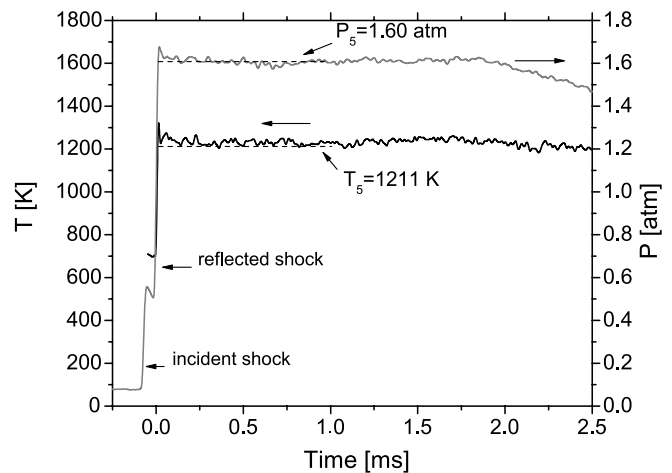


FIGURE 10 Measured temperature and pressure trace during a shock with H_2O –Ar mixture. Initial conditions: $P_1 = 0.08$ atm and $T_1 = 295$ K; incident shock conditions (calculated): $P_2 = 0.46$ atm and $T_2 = 696$ K; reflected shock conditions (calculated): $P_5 = 1.60$ atm and $T_5 = 1211$ K. The decay of pressure and temperature beginning at 1.85 ms is due to arrival of the rarefaction wave

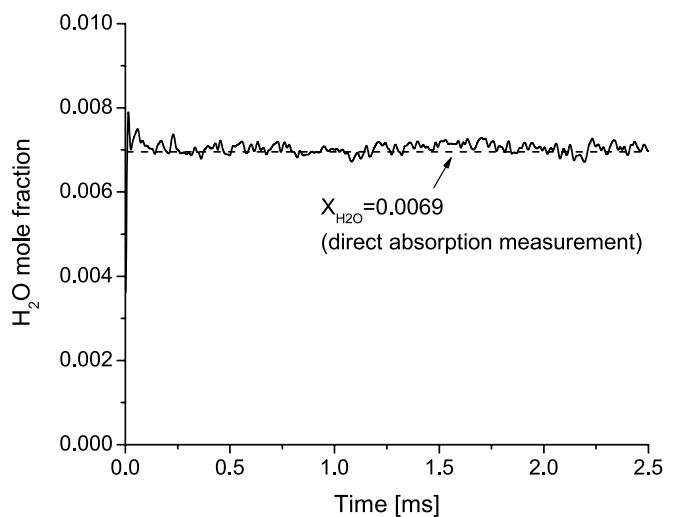


FIGURE 11 Measured water mole fraction by the WMS-2*f* sensor during the same shock as Fig. 10 (H_2O –Ar mixture)

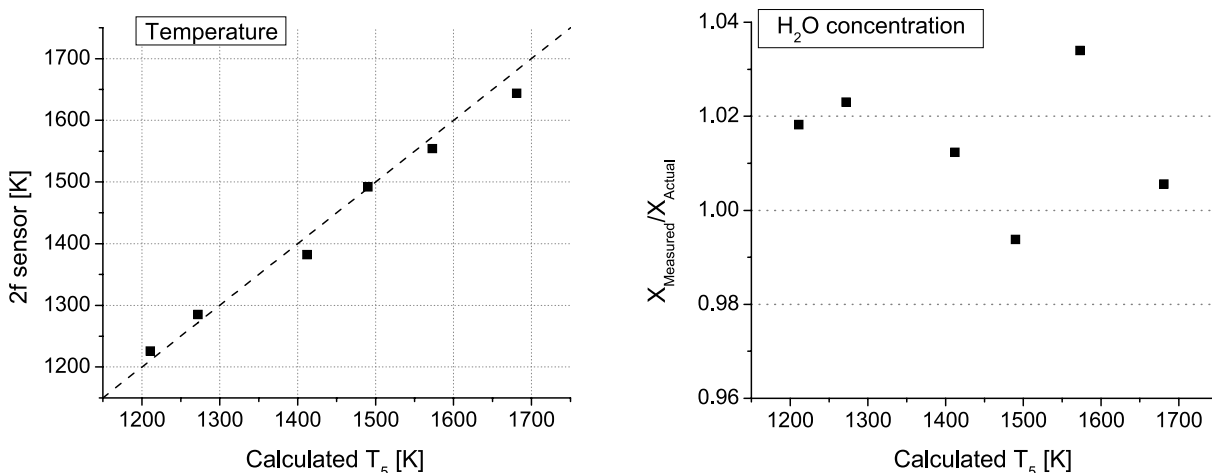


FIGURE 12 Demonstration measurements of the WMS-2*f* sensor in a shock tube with H_2O –Ar mixtures. *Left*: comparison of measured temperature by the WMS-2*f* sensor with calculated T_5 ; *right*: comparison of measured H_2O by the WMS-2*f* sensor with direct absorption measurement before the shock. $P_5 = 1.3$ –1.6 atm, $\sim 0.70\%$ H_2O in Ar, $L = 15.24$ cm

temperature measured by the WMS-2*f* sensor (averaged over the time 0.1–1 ms) with the calculated T_5 . They are in good agreement (within 1.5%) over the tested temperature range of 1200–1700 K. The right-hand panel of Fig. 12 shows the ratio of the H₂O mole fraction measured by the WMS-2*f* sensor (χ_{Measured}) and the mole fraction measured by direct absorption with the laser 1388 nm before the shock (χ_{Actual}). They agree within 1.4% over the tested range. These results validate the sensor accuracy for temperature and H₂O concentration measurements at combustion temperatures, and illustrate the potential for applications in combustion studies with varying temperature and H₂O concentration.

6 Summary

A NIR tunable diode laser absorption sensor based on wavelength modulation spectroscopy with second-harmonic detection is demonstrated for rapid measurements (bandwidth 100 kHz) of temperature and H₂O concentration in shock-heated gases. The sensor is based on TDL absorption of two H₂O transitions near 7185.60 cm⁻¹ and 7154.35 cm⁻¹, which are selected as the optimum line pair (based on design rules) for the target temperature range of 1000–2000 K and pressure range of 1–2 atm. The laser modulation depth for each H₂O transition is optimized to maximize the WMS-2*f* signal for the target test conditions. The fast response of the TDL sensor is achieved by fixing the laser wavelengths near the line center of corresponding H₂O transitions, and set by the digital lock-in bandwidth (currently 100 kHz). Normalization of the WMS-2*f* signal by the 1*f* signal is used to remove the need for calibration and minimize interference from emission, scattering, and beam steering.

The WMS-2*f* sensor is first validated in a controlled laboratory environment (heated static cell) for the temperature range of 500–1200 K ($P = 1$ atm). Temperature measurements are within 1.9% of thermocouple readings, and H₂O concentration measurements are within 1.4% of expected values. Shock tests with non-reactive H₂O–Ar mixtures are then conducted to demonstrate the sensor accuracy and response at higher temperatures (1200–1700 K, $P = 1.3$ – 1.6 atm). Temperature measurements are within 1.5% of calculated values from the ideal shock relations, and H₂O concentration measurements are within 1.4% of expected values. This fast-response WMS-2*f* sensor provides a new diagnostic tool for shock tube experiments and is currently being used to study the thermal decomposition and oxidation of hydrocarbon fuels.

ACKNOWLEDGEMENTS We gratefully acknowledge support from the Air Force Office of Scientific Research (AFOSR) with Dr. Julian Tishkoff as technical monitor, and the Army Research Office (ARO) with Dr. Ralph Anthenien as technical monitor. We would also like to thank Robert D. Cook for assistance with shock tube experiments.

REFERENCES

- 1 I. Glassman, *Combustion* (Academic, San Diego, CA, 1996)
- 2 C.T. Bowman, R.K. Hanson, *J. Phys. Chem.* **83**, 757 (1979)
- 3 R.K. Hanson, D.F. Davidson, in *Handbook of Shock Waves*, ed. by G. Ben-Dor, O. Igra, T. Elperin (Academic, San Diego, CA, 2001), vol. 1, Chap. 5.2
- 4 H.J. Curran, P. Gaffuri, W.J. Pitz, C.K. Westbrook, *Combust. Flame* **114**, 149 (1998)
- 5 D.F. Davidson, R.K. Hanson, *Int. J. Chem. Kinet.* **36**, 510 (2004)
- 6 M.G. Allen, *Meas. Sci. Technol.* **9**, 545 (1998)
- 7 D. Richter, D.G. Lancaster, F.K. Tittel, *Appl. Opt.* **39**, 4444 (2000)
- 8 S.T. Sanders, J.A. Baldwin, T.P. Jenkins, D.S. Baer, R.K. Hanson, *Proc. Combust. Inst.* **28**, 587 (2000)
- 9 H. Teichert, T. Fernholtz, V. Ebert, *Appl. Opt.* **42**, 2043 (2003)
- 10 D.S. Baer, V. Nagali, E.R. Furlong, R.K. Hanson, *AIAA J.* **34**, 489 (1996)
- 11 D.T. Cassidy, J. Reid, *Appl. Opt.* **21**, 1185 (1982)
- 12 J.A. Silver, D.J. Kane, *Meas. Sci. Technol.* **10**, 845 (1999)
- 13 L.C. Philippe, R.K. Hanson, *Appl. Opt.* **32**, 6090 (1993)
- 14 J.T.C. Liu, J.B. Jeffries, R.K. Hanson, *Appl. Phys. B* **78**, 503 (2004)
- 15 J. Wang, M. Maiorov, D.S. Baer, D.Z. Garbuzov, J.C. Connolly, R.K. Hanson, *Appl. Opt.* **39**, 5579 (2000)
- 16 J. Reid, D. Labrie, *Appl. Phys. B* **26**, 203 (1981)
- 17 J.A. Silver, *Appl. Opt.* **31**, 707 (1992)
- 18 T. Aizawa, *Appl. Opt.* **40**, 4894 (2001)
- 19 P. Kluczynski, O. Axner, *Appl. Opt.* **38**, 5803 (1999)
- 20 H. Li, G.B. Rieker, X. Liu, J.B. Jeffries, R.K. Hanson, *Appl. Opt.* **45**, 1052 (2006)
- 21 G.B. Rieker, H. Li, X. Liu, J.T.C. Liu, J.B. Jeffries, R.K. Hanson, M.G. Allen, S.D. Wehe, P.A. Mulhall, H.S. Kindle, A. Kakuho, K.R. Sholes, T. Matsuura, S. Takatani, *Proc. Combust. Inst.* **31**, 3041 (2007)
- 22 T. Fernholtz, H. Teichert, V. Ebert, *Appl. Phys. B* **75**, 229 (2002)
- 23 T. Iseki, H. Tai, K. Kimura, *Meas. Sci. Technol.* **11**, 594 (2000)
- 24 R.T. Wainner, B.D. Green, M.G. Allen, M.A. White, J. Stafford-Evans, R. Naper, *Appl. Phys. B* **75**, 249 (2002)
- 25 R. Arndt, *J. Appl. Phys.* **36**, 2522 (1965)
- 26 X. Zhou, X. Liu, J.B. Jeffries, R.K. Hanson, *Meas. Sci. Technol.* **14**, 1459 (2003)
- 27 X. Zhou, J.B. Jeffries, R.K. Hanson, *Appl. Phys. B* **81**, 711 (2005)
- 28 X. Liu, J.B. Jeffries, R.K. Hanson, K.M. Hincley, M.A. Woodmansee, *Appl. Phys. B* **82**, 469 (2006)
- 29 X. Zhou, X. Liu, J.B. Jeffries, R.K. Hanson, *Meas. Sci. Technol.* **16**, 2437 (2005)
- 30 L.S. Rothman, D. Jacquemart, A. Barbe, D.C. Benner, M. Birk, L.R. Brown, M.R. Carleer Jr., C. Chackerian, K. Chance, L.H. Couderc, V. Dana, V.M. Devi, J.-M. Flaud, R.R. Gamache, A. Goldman, J.-M. Hartmann, K.W. Jucks, A.G. Maki, J.-Y. Mandin, S.T. Massie, J. Orphal, A. Perrin, C.P. Rinsland, M.A.H. Smith, J. Tennyson, R.N. Tolchenov, R.A. Toth, J. Vander Auwera, P. Varanasi, G. Wagner, *J. Quant. Spectrosc. Radiat. Transf.* **96**, 139 (2005)
- 31 H. Li, A. Farooq, J.B. Jeffries, R.K. Hanson, *J. Quant. Spectrosc. Radiat. Transf.*, DOI: 10.1016/j.jqsrt.2007.05.008 (2007)
- 32 R.H. Dicke, *Phys. Rev.* **89**, 472 (1953)
- 33 L. Galatry, *Phys. Rev.* **122**, 1218 (1961)
- 34 P.L. Varghese, R.K. Hanson, *Appl. Opt.* **23**, 2376 (1984)
- 35 G.B. Rieker, H. Li, X. Liu, J.B. Jeffries, R.K. Hanson, M.G. Allen, S.D. Wehe, P.A. Mulhall, H.S. Kindle, *Meas. Sci. Technol.* **18**, 1195 (2007)
- 36 S. Song, R.K. Hanson, C.T. Bowman, D.M. Golden, *Proc. Combust. Inst.* **28**, 2403 (2000)
- 37 V. Vasudevan, D.F. Davidson, R.K. Hanson, *J. Phys. Chem. A* **109**, 3352 (2005)
- 38 X. Liu, X. Zhou, J.B. Jeffries, R.K. Hanson, *J. Quant. Spectrosc. Radiat. Transf.* **103**, 565 (2007)